Rate-Adaptive Modulation and Coding for Optical Fiber Transmission Systems

Gwang-Hyun Gho and Joseph M. Kahn, *Fellow, IEEE*

***Abstract*—We propose a rate-adaptive optical transmission scheme using variable-rate forward error correction (FEC) codes and variable-size constellations at a fixed symbol rate, quantifying how achievable bit rates vary with distance. The scheme uses serially concatenated Reed–Solomon codes and an inner repetition code to vary the code rate, combined with single-carrier polarization-multiplexed M-ary quadrature amplitude modulation with variable M and digital coherent detection. Employing $M = 4, 8, 16$, the scheme achieves a maximum bit rate of 200 Gb/s in a nominal 50-GHz channel bandwidth. A rate adaptation algorithm uses the signal-to-noise ratio (SNR) or the FEC decoder input bit-error ratio (BER) estimated by a receiver to determine the FEC code rate and constellation size that maximizes the information bit rate while yielding a target FEC decoder output BER and a specified SNR margin. We simulate single-channel transmission through long-haul fiber systems with or without inline chromatic dispersion compensation, incorporating numerous optical switches, evaluating the impact of fiber nonlinearity and bandwidth narrowing. With zero SNR margin, we achieve bit rates of 200/100/50 Gb/s over distances of 640/2080/3040 km and 1120/3760/5440 km in dispersion-compensated and dispersion-uncompensated systems, respectively. Compared to an ideal coding scheme, the proposed scheme exhibits a performance gap ranging from about 6.4 dB at 640 km to 7.6 dB at 5040 km in compensated systems, and from about 6.6 dB at 1120 km to 7.5 dB at 7600 km in uncompensated systems. We present limited simulations of three-channel transmission, showing that interchannel nonlinearities decrease achievable distances by about 10% and 7% for dispersion-compensated and dispersion-uncompensated systems, respectively.**

***Index Terms*—Adaptive modulation, coherent detection, forward error correction (FEC), information rates, optical fiber communication, quadrature amplitude modulation, variable-rate codes.**

I. Introduction

EARLY wireline and wireless communication systems transmitted typically at a fixed information bit rate, using a fixed forward error correction (FEC) code, modulation order, and transmitted signal power. Many recent systems, including asymmetric digital subscriber lines, WiMAX, and high-speed downlink packet access, adapt these link parameters depending on channel conditions (often time varying), trading off bit rate (and thus spectral efficiency) for robustness. Previous optical transmission systems, such as those based on synchronous optical networking and synchronous digital hierarchy, employed fixed bit rates. As Ethernet-based systems are deployed in large-scale IP networks [1], transponders using coherent detection and DSP will enable higher bit rates and spectral efficiencies, and could also support rate-adaptive transmission, with bit rates negotiated between routers and transponders. Optical switches, such as reconfigurable optical add-drop multiplexers (ROADMs), make it possible to route signals optically over longer distances but add loss and can limit signal bandwidth, all of which can make signal quality more variable. Rate-adaptive transmission could help improve network robustness, flexibility, and throughput. Although present standardization efforts for optical transport networks are concentrated on transmitting client data at fixed rates [2], rate-adaptive modulation and coding may merit consideration for future networks.

Variable-rate transmission using variable-rate codes with a *fixed constellation* (4-QAM) was proposed in [3], where its performance was evaluated for single-channel transmission in systems using inline dispersion compensation. In this paper, we evaluate variable-rate codes with *variable-size constellations* (4-, 8-, and 16-QAM). We present extensive studies of single-channel transmission in systems with or without inline chromatic dispersion (CD) compensation, and some limited studies of wavelength-division-multiplexed (WDM) transmission to evaluate the impact of interchannel nonlinearities. Considering that rate-adaptive transmission can significantly extend transmission distances, we also study the implications for relevant hardware requirements, namely equalizer filter lengths and laser linewidths.

This paper is organized as follows. In Section II, we describe the proposed scheme using variable-rate codes and variable-size constellations, and a rate adaptation algorithm that uses measured signal-to-noise ratio (SNR) or FEC decoder input bit-error ratio (BER) to determine the maximum supportable information bit rate. In Section III, we describe simulations of the rate-adaptive scheme in a model terrestrial network. In Section IV, we present simulation results, including achievable information bit rates as a function of distance, with or without CD compensation. In Section V, we discuss the observed trend of SNR versus distance and compare the performance of the proposed scheme to information-theoretic limits. We also discuss the results of three-channel simulations. We present conclusions in Section VI. In the Appendix, we discuss error-probability calculations.

Manuscript received May 06, 2011; revised December 17, 2011, February 11, 2012; accepted February 23, 2012. Date of publication February 28, 2012; date of current version April 09, 2012. This work was supported in part by a Google Research Award.

G.-H. Gho was with the Department of Electrical Engineering, Stanford University, Stanford, CA 94305-4088 USA. He is now with Qualcomm Inc., Santa Clara, CA 95051 USA (e-mail: ggho@alumni.stanford.edu).

J. M. Kahn is with the E. L. Ginzton Laboratory, Department of Electrical Engineering, Stanford University, Stanford, CA 94305-4088 USA (e-mail: jmk@ee.stanford.edu).

Digital Object Identifier 10.1109/JLT.2012.2189435

0733-8724/$31.00 © 2012 IEEE

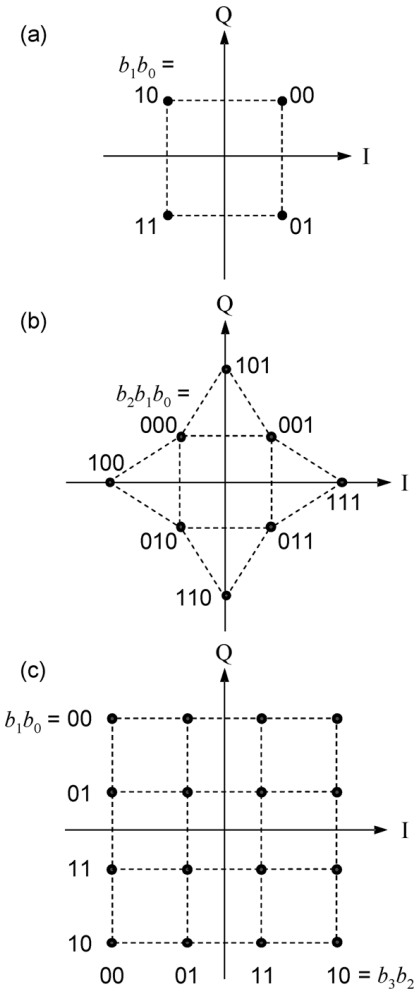

Fig. 1. QAM constellations with bit-to-symbol mappings. (a) Square 4-QAM. (b) Cross 8-QAM. (c) Square 16-QAM.

II. Rate-Adaptive Modulation and Coding Scheme

A. Variable-Size Constellations

We use PM-M-QAM with modulation orders $M = 4, 8, 16$. The constellations for the various M are shown in Fig. 1, where the signal amplitudes have been scaled so the average energy is the same for all M. Gray mapping is used for 4- and 16-QAM square constellations. The bit mapping in [4] is used for the 8-QAM cross constellation, because we verified it performs best in the presence of nonlinearity (although it is not optimal on an AWGN channel [5]).

B. Variable-Rate FEC Coding Scheme

The FEC scheme uses serially concatenated Reed–Solomon (RS) codes, referred to as RS–RS codes, in GF(2^8)[1]. A family of variable-rate RS–RS codes is constructed by puncturing and shortening a mother code that has a rate in the middle of the desired range, as described in [3], trading off hardware complexity and performance. Higher rate and lower rate codes are generated by puncturing and shortening the inner RS code of the mother code, respectively. Hard-decision decoding of the RS–RS code is employed. The rates and performance of the constructed codes are shown in Fig. 2, where n and k indicate the length in bytes of the code word and message word, respectively, and $P_{b,\mathrm{in}}$ and $P_{b,\mathrm{out}}$ are input and output BERs of the RS–RS decoder. The curves in Fig. 2 have been calculated analytically assuming independent errors and no decoding failures [6]. The highest rate code, with code rate 0.8765, offers a net coding gain of about 7.6 dB at a decoded BER of 10^{-13}, comparable to second-generation FEC codes [7].

[1]This is a correction to GF(8) stated in [3].

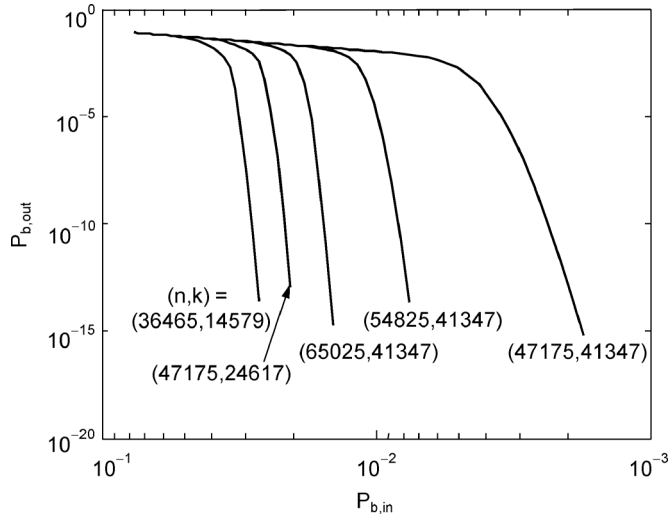

Fig. 2. Performance of serially concatenated RS–RS codes with five different rates, in terms of input and output BERs of the RS–RS decoder.

To compensate for the diminishing gain obtained by hard-decision decoding of RS–RS codes at low rates, as in [3], an inner repetition code is added, with repetition factor f_R ranging from 1 to 4. While suboptimal, repetition coding allows operation at very low SNR with minimal increase in complexity. Repetitions are separated by 66 symbols, to make the scheme compatible with the 64b/66b line coding used in 10 Gb Ethernet and proposed for 100 Gb Ethernet. In order to minimize noise correlation between repeated symbols caused by fiber nonlinearity and CD, permutation of repeated symbols is performed, as in [3]. Soft-decision decoding of the repetition code is employed.

We assume that line encoding, RS–RS encoding, and repetition encoding are performed on a single serial bit stream, after which, blocks of $66f_R$ bits are permuted and mapped in round-robin fashion to the $2\log_2 M$ tributaries of the PM-M-QAM signal. In order to minimize noise correlation between repeated symbols caused by fiber nonlinearity, when $f_R > 1$, the second, third, and fourth repetition of a block are permuted using different matrices as in [3]. The symbol mapping of FEC-encoded and permuted bits is illustrated in Fig. 3, where x and y are two polarizations and the bit index b_i is defined in Fig. 1.

C. Rate Adaptation Algorithm

Given a symbol rate R_s, an RS–RS code rate $r_C = k/n$, a repetition code rate $r_R = 1/f_R$, a line code rate r_L, and a modulation order M, the information bit rate R_b can be calculated as

$$R_b = 2r_L r_C r_R R_s \log_2 M \tag{1}$$

assuming PM transmission.

The achievable bit rate R_b is quantized into multiple segments $R_{b,i}, i = 1, 2, \ldots, N_s$, where $R_{b,i} < R_{b,i+1}$. Each

$R_{b,i}$ can be represented by a set of transmission parameters $(M, f_R, r_C)_i$, commonly referred to as a *mode*. For each transmission mode, we define a threshold value for channel state information (CSI), at which $(M, f_R, r_C)_i$ can achieve a target decoder output BER, $P_{b,\mathrm{out,req}}$, on an additive white Gaussian noise (AWGN) channel. The controller runs a rate adaptation algorithm based on CSI that is estimated at the receiver and reported to the transmitter. The transmitter monitors variations of reported CSI, and adjusts the RS–RS and repetition code rates and constellation size to maximize R_b, while achieving $P_{b,\mathrm{out,req}}$. We consider two possible choices for CSI: 1) *SNR*, which is the SNR per symbol estimated at the derepeater soft input, or 2) $P_{b,\mathrm{in}}$, which is the BER of hard decisions measured at the derepeater output (RS–RS decoder input). We design the rate adaptation algorithm such that it can provide an arbitrary specified SNR margin.

A rate adaptation algorithm using *SNR* as CSI may not reliably yield the highest feasible information bit rate when SNR is not an accurate predictor of $P_{b,\mathrm{out}}$, but it is easiest to understand, so it is described first. Fig. 4 shows information bit rates and threshold values of *SNR* for different combinations of (M, f_R, r_C) on an AWGN channel, where the highest bit rate $R_b = 200$ Gb/s is achieved using (1) and assuming $R_s = 29.4152$ Gsymb/s, $r_L = 64/66, r_R = 1, r_C$ for Code 1, and $M = 16$. The plots for $f_R = 1$ are obtained assuming $P_{b,\mathrm{out,req}} = 10^{-15}$ and using Fig. 2, (1), and the following relationships between *SNR* and $P_{b,\mathrm{in}}$ for a QAM constellation on an AWGN channel [8]:

$$P_{s,\mathrm{in}} \le \begin{cases} 4 \cdot \left(1 - \frac{1}{\sqrt{M}}\right) Q\left(\sqrt{\frac{3}{M-1} SNR}\right), & M = 4, 16 \\ 3 \cdot Q\left(\sqrt{0.423 SNR}\right), & M = 8 \end{cases} \tag{2}$$

$$P_{b,\mathrm{in}} \approx \begin{cases} \frac{1}{\log_2 M} P_{s,\mathrm{in}}, & M = 4, 16 \\ \frac{1.375}{3} P_{s,\mathrm{in}}, & M = 8 \end{cases} \tag{3}$$

where $P_{s,\mathrm{in}}$ is the upper bound on the symbol-error ratio (SER) at FEC decoder input considering only nearest neighbors, and $P_{b,\mathrm{in}}$ is the decoder input BER using the bit mappings shown in Fig. 1. In (2), the *Q*-function is defined as

$$Q(x) = \frac{1}{2} \cdot \mathrm{erfc}\left(\frac{x}{\sqrt{2}}\right) \tag{4}$$

where $\mathrm{erfc}(\cdot)$ is the complementary error function. The plots for $f_R \ge 2$ in Fig. 4 are computed from those for $f_R = 1$ by dividing R_b by f_R and subtracting $10 \log_{10}(f_R)$ from the threshold value of *SNR*. The filled (M, f_R, r_C) combinations represent a possible choice of transmission modes, showing one example that quantizes the range of R_b and CSI values into roughly equally spaced segments. Denoting the threshold *SNR* value for mode i on an AWGN channel by $SNR_{th,i}$, a threshold *SNR* value for mode i with margin μ dB is defined as $SNR_{th,i,\mu} = SNR_{th,i} + \mu$ dB as in [3].

An algorithm using $P_{b,\mathrm{in}}$ as CSI is perhaps harder to understand (though not necessarily harder to implement), but can reliably yield the highest feasible information bit rate, since $P_{b,\mathrm{in}}$ is an accurate predictor of $P_{b,\mathrm{out}}$ for a hard-decision RS–RS decoder. $P_{b,\mathrm{in}}$ can be estimated by the decoder from the number of bit errors corrected in decoding. Assuming a highest achievable bit rate $R_b = 200$ Gb/s, Fig. 5 shows information bit rates and threshold values of $P_{b,\mathrm{in}}$ for different combinations of (M, f_R, r_C). The plots for $f_R = 1$ are computed assuming $P_{b,\mathrm{out,req}} = 10^{-15}$ and using Fig. 2 and (1)–(3). The plots for $f_R \ge 2$ are computed from those for $f_R = 1$ by dividing R_b by f_R. A threshold value of $P_{b,\mathrm{in}}$ for mode i with margin μ dB, $P_{b,\mathrm{in,th},i,\mu}$, is defined as the value of $P_{b,\mathrm{in}}$ for $(M, f_R, r_C)_i$ at $SNR_{th,i} + \mu$ dB on an AWGN channel.

A pseudocode for the rate adaptation algorithm using *SNR* or $P_{b,\mathrm{in}}$ as CSI is given as follows.

1) Initialize parameters to the highest rate mode.
   a) Initialize mode: $(M, f_R, r_C)_i \rightarrow (M, f_R, r_C)_{\mathrm{Ns}}$.
   b) Initialize up/down counters: $C_{\mathrm{up}} = C_{\mathrm{down}} = 0$.

2) Check if rate change is necessary:
   a) if *CSI* satisfies $CSI_{th,i+1}\{\Delta_i, \mu_{\mathrm{up}}\}$
      i) $C_{\mathrm{up}} = C_{\mathrm{up}} + 1$
      ii) if $C_{\mathrm{up}} \ge N_{\mathrm{up}}, (M, f_R, r_C)_i \rightarrow (M, f_R, r_C)_{i+1}$

   b) elseif *CSI* does not satisfy $CSI_{th,i}\{\Delta_i, \mu_{\mathrm{down}}\}$
      i) $C_{\mathrm{down}} = C_{\mathrm{down}} + 1$
      ii) if $C_{\mathrm{down}} \ge N_{\mathrm{down}}, (M, f_R, r_C)_i \rightarrow (M, f_R, r_C)_{i-1}$

   c) else
      i) $C_{\mathrm{up}} = C_{\mathrm{down}} = 0$
      ii) $(M, f_R, r_C)_i \rightarrow (M, f_R, r_C)_i$

3) Go to step 2.

$CSI_{th,i}\{\Delta_i, \mu\}$ denotes a threshold CSI value for mode i considering SNR penalty Δ_i and SNR margin μ. The parameters μ_{up} and μ_{down} are SNR margins when changing rate up and down, respectively, and N_{up} and N_{down} are counters when changing rate up and down, respectively. Since *SNR* may not be a sufficiently accurate predictor of $P_{b,\mathrm{in}}$, as in [3], we introduce SNR penalty parameters Δ_i, which quantify the increase in *SNR* required to achieve a specified $P_{b,\mathrm{in}}$ when using $(M, f_R, r_C)_i$, as compared to the AWGN case. We note that SNR penalty parameters are not required when using $P_{b,\mathrm{in}}$ as CSI [3].

III. System Simulations

We have evaluated the rate-adaptive transmission scheme in the model long-haul system shown in Fig. 6. In most of the study, we simulated a single channel with center wavelength of 1550 nm and nominal 50-GHz bandwidth, suitable for a WDM system with 50-GHz channel spacing. The modulation is single-carrier PM-M-QAM using nonreturn-to-zero (NRZ) pulses at a symbol rate $R_s = 29.4152$ Gsymb/s. We used the same models for the modulator, drive waveform, and transmit filter as described in [3]. We assume line coding at rate $r_L = 64/66$, yielding an information bit rate $R_b = 200$ Gb/s for the highest overall code rate $r_C r_R$ and $M = 16$.

The fiber network comprises multiple 80-km spans of standard single-mode fiber (SMF). In dispersion-compensated systems, dispersion-compensating fiber (DCF) is used to precompensate CD down to 3.1% residual dispersion per span (RDPS). The parameters for SMF and DCF are summarized in Table I. We use the same parameters for inline amplifiers, ROADMs (inserted at every third span), multiplexer, and demultiplexer as provided in [3].

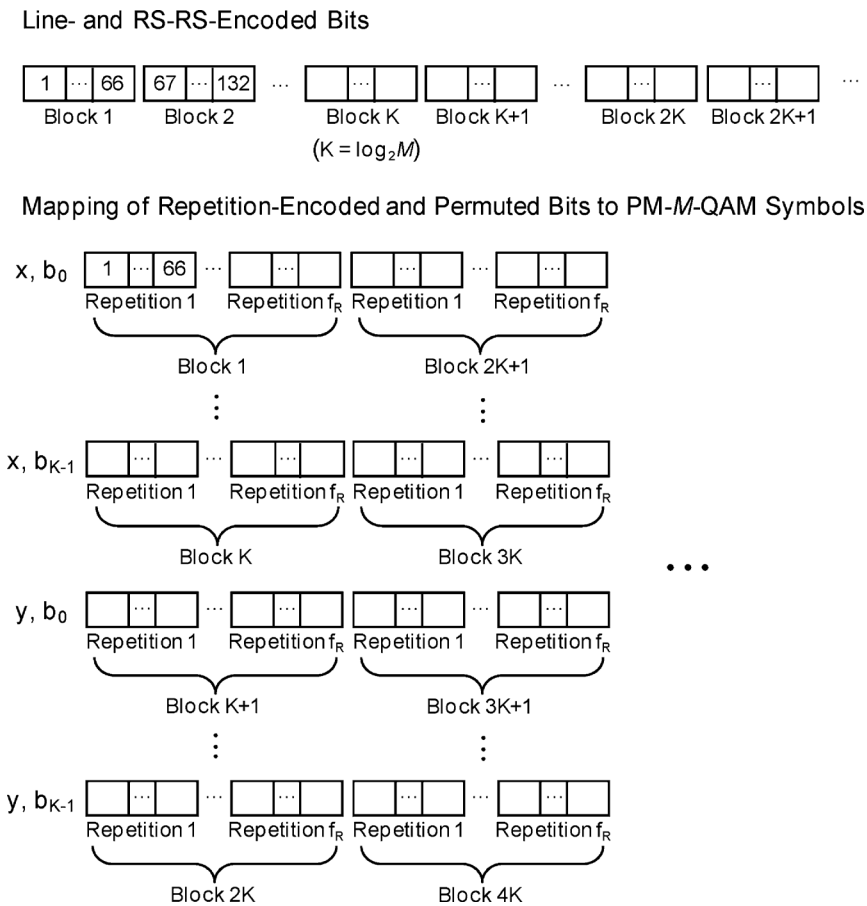

Fig. 3. Mapping of FEC-encoded and permuted bits to PM-M-QAM symbols assumed in model system, where x and y are two polarizations and the bit index b_i follows the definition in Fig. 1.

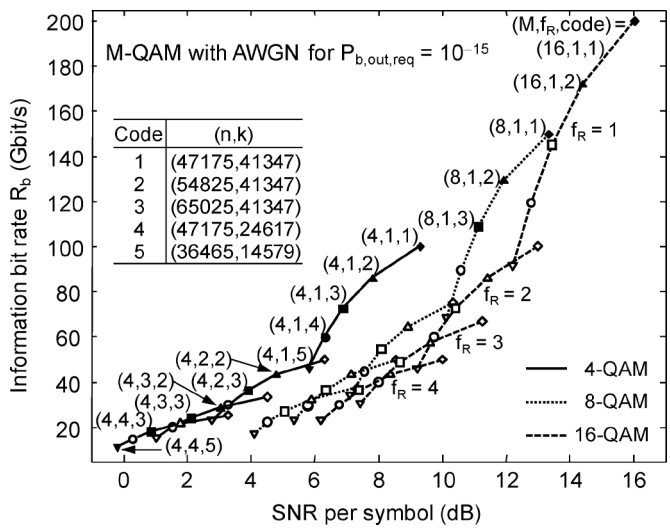

Fig. 4. Information bit rate versus threshold SNR per symbol for PM-M-QAM on AWGN channel. Information bit rates are computed using (1), while SNR values are computed by combining (2), (3), and Fig. 2. The set of filled (M, f_R, code) combinations represents a possible choice of modes for rate-adaptive transmission.

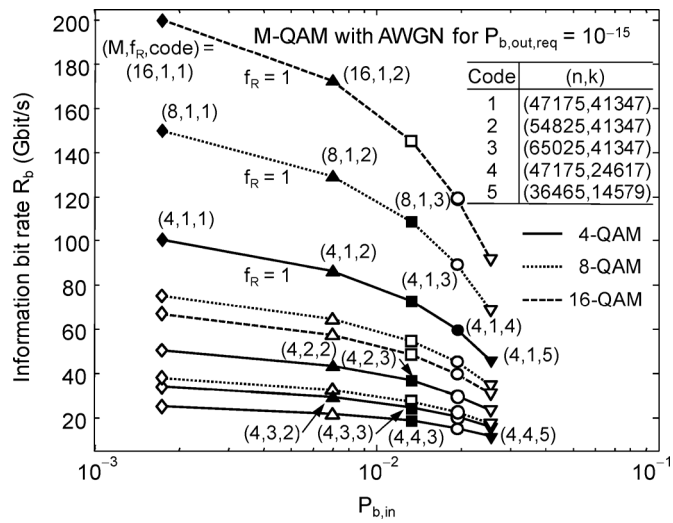

Fig. 5. Information bit rate versus threshold $P_{b,\mathrm{in}}$ for PM-M-QAM on AWGN channel. Information bit rates are computed using (1), while $P_{b,\mathrm{in}}$ values are computed by combining (2), (3), and Fig. 2. The set of filled (M, f_R, code) combinations represents a possible choice of modes for rate-adaptive transmission.

The receiver employs a fifth-order Butterworth antialiasing filter of 3-dB bandwidth R_s, samples at a rate of $2R_s$ complex samples per polarization and performs digital compensation of CD and polarization-mode dispersion using finite impulse response time-domain filtering, as described in [9]. We found that

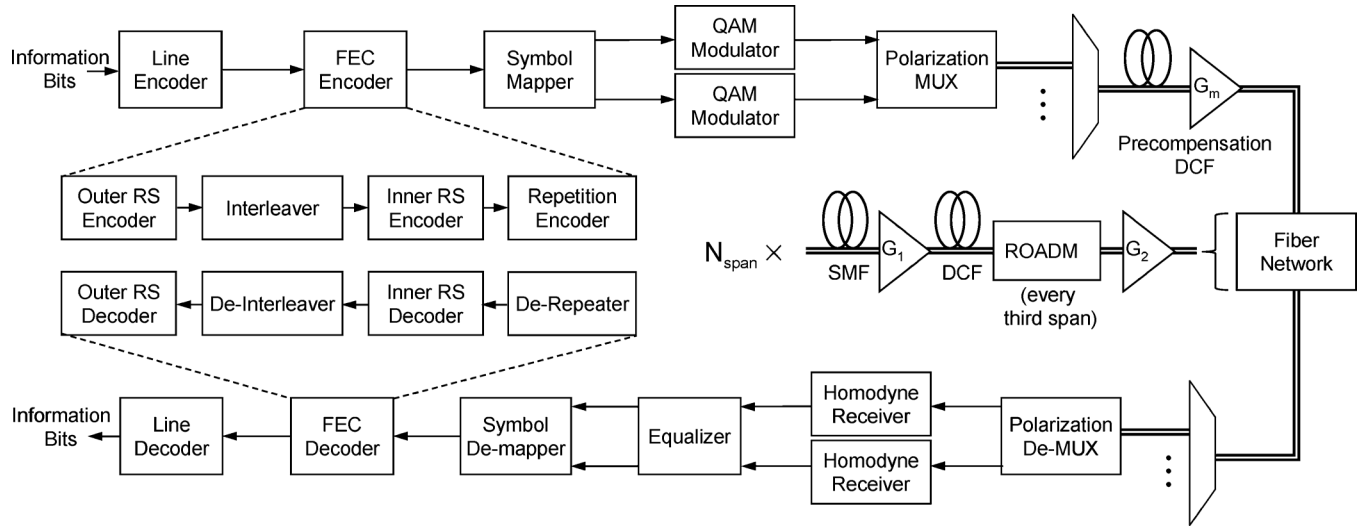

Fig. 6. Model long-haul optical system that consists of line and FEC encoder/decoder, equalizer, PM-M-QAM modulator/demodulator, dispersion precompensation fiber, and multiple spans. Note that precompensation and inline DCFs are bypassed for simulation of dispersion-uncompensated system.

TABLE I
PARAMETERS FOR SMF AND DCF. DCF IS OMITTED FROM DISPERSION-UNCOMPENSATED SYSTEMS

Parameter	Value	Unit
SMF length per span	80	km
Inline DCF length per span	15.5	km
Pre-compensation DCF length	6	km
SMF loss coefficient	0.25	dBm/km
DCF loss coefficient	0.6	dBm/km
SMF CD coefficient	17	ps/(nm·km)
DCF CD coefficient	−85	ps/(nm·km)
SMF/DCF PMD coefficient	0.1	ps/km$^{1/2}$
SMF nonlinear coefficient	0.0012	W^{-1}m^{-1}
DCF nonlinear coefficient	0.0053	W^{-1}m^{-1}

in order to render residual intersymbol interference (ISI) negligible, the number of equalizer taps optimized at each transmission distance is

$$N = 2 \cdot 2\pi(|\beta_2|L)_{\text{eff}} R_s^2 (M/K) + 7 \approx 12.6(|\beta_2|L)_{\text{eff}} R_s^2 (M/K) + 7. \quad (5)$$

This is about twice the number given in [9], which would result in a 2-dB penalty from residual ISI. The first term of (5) corresponds to the group delay spread from uncompensated CD, which varies with transmission distance, while the second term corresponds to the group delay spread from the transmitter and receiver filters, which is independent of transmission distance. The effective value of the product $|\beta_2|L$ can be computed as

$$(|\beta_2|L)_{\text{eff}} = \sum_{k=1}^{N_{\text{span}}} |\beta_{2,\text{SMF}} L_{k,\text{SMF}} + \beta_{2,\text{DCF}} L_{k,\text{DCF}}| = N_{\text{span}} |\beta_{2,\text{SMF}} L_{k,\text{SMF}} + \beta_{2,\text{DCF}} L_{k,\text{DCF}}| \quad (6)$$

where N_{span} is the number of spans, $\beta_{2,\text{SMF}}$ and $\beta_{2,\text{DCF}}$ are the CD parameters of SMF and DCF, respectively, and $L_{k,\text{SMF}}$ and $L_{k,\text{DCF}}$ are the lengths of SMF and DCF in the kth span, respectively. Using (5), Fig. 7 shows that the dispersion-uncompensated system requires more filter taps than the compensated system, by more than an order of magnitude for $L > 1000$ km.

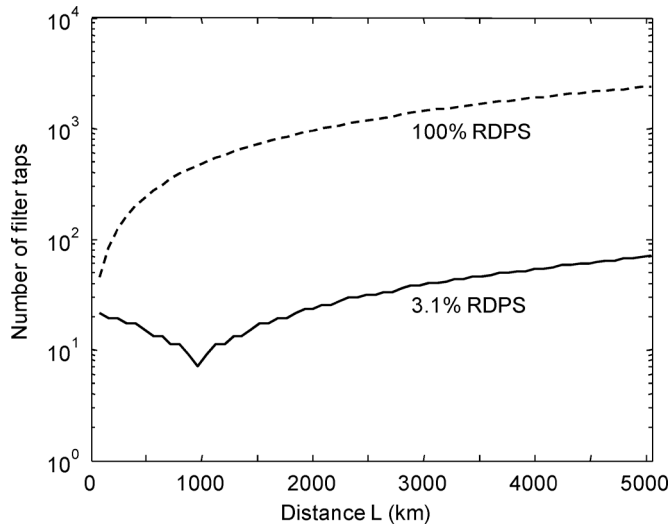

Fig. 7. Number of filter taps employed in the equalizer based on the formula (5), for dispersion-compensated and dispersion-uncompensated systems. For $L > 1000$ km, an uncompensated system requires more than ten times as many filter taps as a compensated system.

Signal propagation is simulated by numerical integration of the vector nonlinear Schrödinger equation by the split-step Fourier method [10].

We estimate $P_{b,\text{in}}$ at the derepeater output using two different methods, depending on the confidence level obtained by error counting. In the first regime, we estimate $P_{b,\text{in}}$ by error counting. We define $P_{b,\text{in},95,M}, M = 4, 8, 16$, to be the value of the estimate of $P_{b,\text{in}}$ such that the true value does not exceed 130% of the estimate with 95% confidence. We find that $P_{b,\text{in},95,4} = 9.1 \times 10^{-4}, P_{b,in,95,8} = 6.2 \times 10^{-4}$ and $P_{b,\text{in},95,16} = 4.5 \times 10^{-4}$. At least for estimated values of $P_{b,\text{in}}$ down to $P_{b,\text{in},95,M}$, we simulate a sufficient number of symbols to obtain the specified confidence level. In this

regime, we find that the uncertainty in $P_{b,\mathrm{in}}$ corresponds to 0.2 dB uncertainty in SNR. In the second regime, when $P_{b,\mathrm{in}}$ estimated by error counting is below $P_{b,\mathrm{in},95,M}$, we estimate noise standard deviations and compute $P_{b,\mathrm{in}}$ as described in the Appendix, in order to reduce simulation time for very low values of $P_{b,\mathrm{in}}$. We estimate that the BER computation method in the Appendix yields uncertainties in $P_{b,\mathrm{in}}$ corresponding to SNR uncertainties of 0.18, 0.56, and 0.38 dB for $M = 4, 8$, and 16, respectively.

At each transmission distance, and for each repetition factor f_R, the launched power is optimized with 1 dB resolution, to minimize the value of $P_{b,\mathrm{in}}$ estimated using the two methods described in the previous paragraph. We have found that in cases when both methods have been used, they result in the same optimized power in about 80% of the cases, and only a 1-dB difference in the remaining cases.

IV. Simulation Results

In order to evaluate the rate-adaptive scheme, at each transmission distance, for each modulation order, and for each repetition factor, after the transmit power is optimized, the received SNR per symbol and decoder input BER are recorded. The SNR per symbol is estimated by calculating the ratio between the average symbol power and the noise variance, which is empirically measured at the derepeater input or output.

Fig. 8 shows the SNR per symbol observed at the derepeater output versus transmitted power P_t for various repetition factors $f_R = 1, 2, 3, 4$, for a representative transmission distance for each modulation order, with and without dispersion compensation. In Fig. 8(a), for $M = 4$, we observe improvements in SNR of 2.9–3.0, 4.5–4.8, and 5.7–6.0 dB for $f_R = 2, 3, 4$ as compared to $f_R = 1$, which are close to the full repetition gains expected for AWGN. Fig. 8(b) and (c) shows improvements in SNR of 2.6–2.8, 4.0–4.2, and 5.0–5.2 dB for $f_R = 2, 3, 4$ for $M = 8$, and 2.5–2.7, 4.0–4.2, and 5.1–5.3 dB for $M = 16$. For multilevel modulations, the observed improvement in SNR is less than expected for AWGN, presumably because they are more sensitive to fiber nonlinearity.

We have employed the rate adaptation algorithm of Section II-C, using $P_{b,\mathrm{in}}$ as CSI, and using all possible transmission modes in Fig. 5. We assume a required FEC decoder output BER $P_{b,\mathrm{out,req}} = 10^{-15}$, SNR margins $M_{\mathrm{up}} = M_{\mathrm{down}} = 0, 1, \ldots, 5$ dB, and counter parameters $N_{\mathrm{up}} = N_{\mathrm{down}} = 1$ (because we assume static channel conditions). Fig. 9(a) and (b) presents achievable information bit rates with and without inline dispersion compensation, respectively, as a function of transmission distance. In dispersion-compensated systems, with zero margin, a bit rate $R_b = 200$ Gb/s can be realized up to 640 km, with the achievable rate decreasing by approximately a factor of two for every additional 1000 km. In dispersion-uncompensated systems, with zero margin, a bit rate $R_b = 200$ Gb/s can be realized up to 1120 km, with the achievable rate decreasing by approximately a factor of two for every additional 2000 km.

We evaluated $P_{b,\mathrm{in}}$ as described in Section III. We find that the uncertainty of $P_{b,\mathrm{in}}$ (either measured by error counting above $P_{b,\mathrm{in},95,M}$ or computed as described in the Appendix below $P_{b,\mathrm{in},95,M}$) may result in a reduced transmission distance by at most one span for dispersion-compensated system, but the penalty may increase to two spans for uncompensated systems at distances above 5000 km.

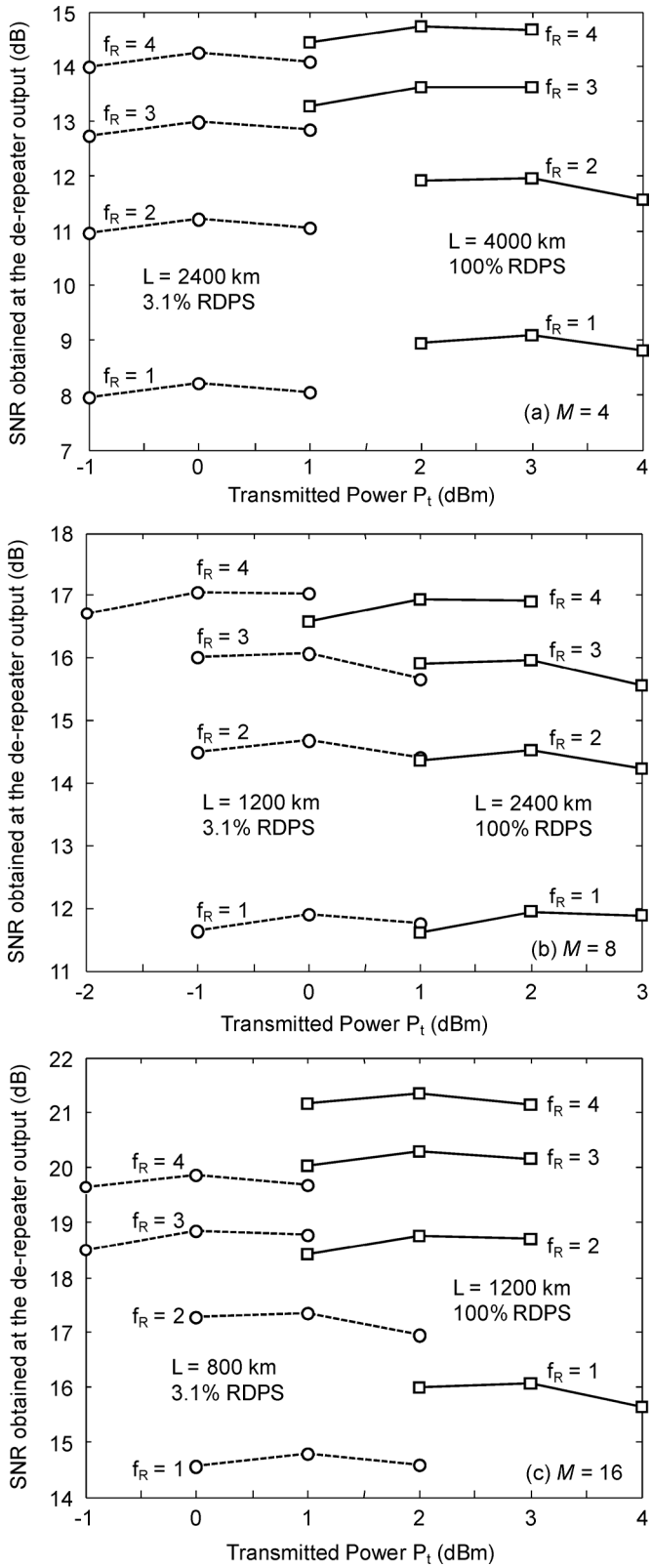

Fig. 8. SNR observed at derepeater output (RS–RS decoder input) as a function of transmitted power, for various repetition factors, with and without dispersion compensation. (a) 4-QAM: $L = 2400$ km and 4000 km. (b) 8-QAM: $L = 1200$ km and 2400 km. (c) 16-QAM: $L = 800$ km and 1200 km.

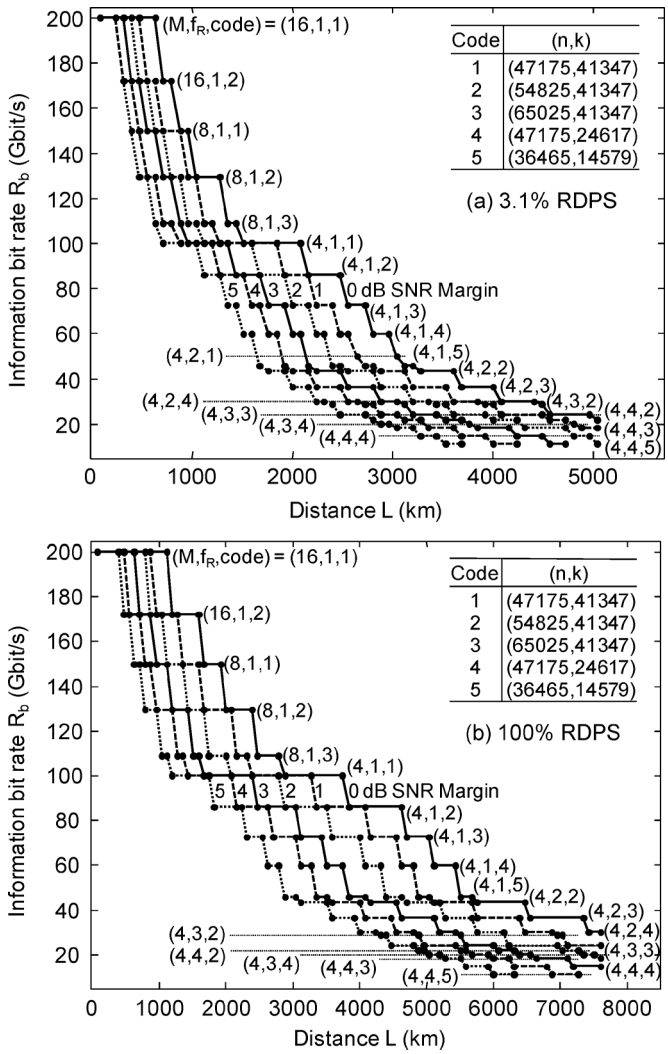

Fig. 9. Achievable information bit rates versus transmission distance for different SNR margins. The set (M, f_R, code) denotes the modulation order, repetition factor and type of RS–RS code. (a) Dispersion-compensated system. (b) Dispersion-uncompensated system.

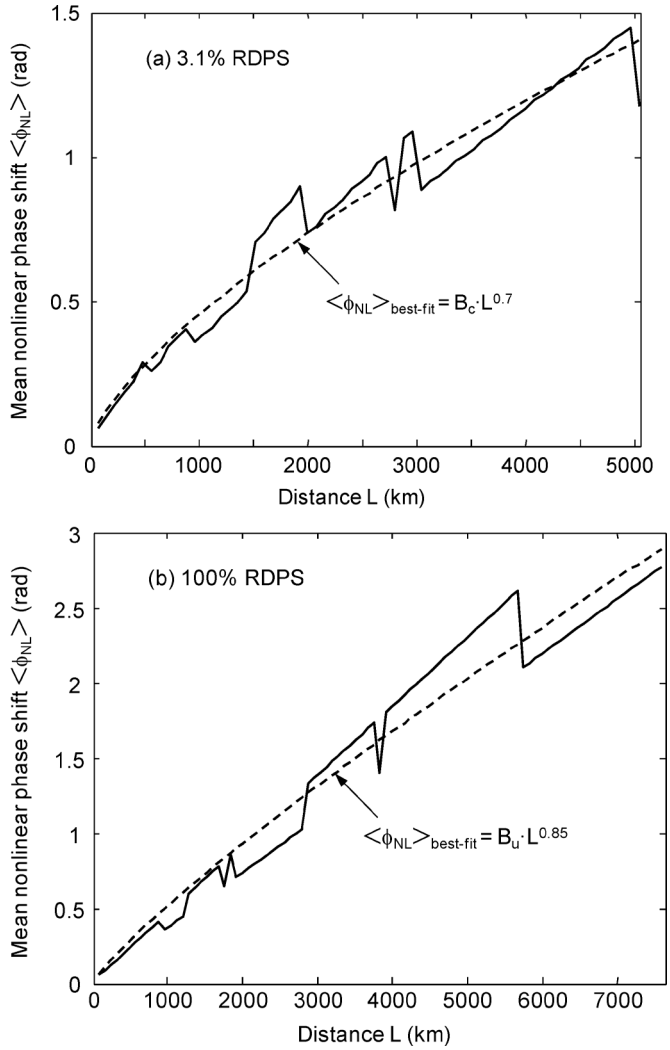

Fig. 10. Mean nonlinear phase shift values computed at optimized launched power levels at repetition factor $f_R = 1$, and fitted by a power law of the form (7). (a) Dispersion-compensated system. (b) Dispersion-uncompensated system.

V. Discussion

In this section, we examine how the optimized mean nonlinear phase shift and SNR in the model system scale with transmission distance, and estimate the performance gap between the proposed rate-adaptive scheme and an ideal coding scheme achieving information-theoretic limits. We also address laser linewidth requirements. Then, we assess how achievable information bit rates are affected by interchannel nonlinearity in WDM systems.

After optimizing the transmitted power P_t, we computed the resulting mean nonlinear phase shift $\langle\phi_{\mathrm{NL}}\rangle$ using [3, eq. (11)]. Optimized values of $\langle\phi_{\mathrm{NL}}\rangle$ versus transmission distance L for unit repetition factor, $f_R = 1$ are shown in Fig. 10(a) and (b) for dispersion-compensated and dispersion-uncompensated systems, respectively. We observe that $\langle\phi_{\mathrm{NL}}\rangle$ approximately follows the power laws:

$$\langle\phi_{\mathrm{NL}}\rangle_{\mathrm{best-fit}} = \begin{cases} B_c \cdot L^{0.7}, & 3.1\%\ \mathrm{RDPS} \\ B_u \cdot L^{0.85}, & 100\%\ \mathrm{RDPS} \end{cases} \tag{7}$$

where the constants B_c, B_u and the exponents of L have been found by curve fitting. In the dispersion-compensated system, $\langle\phi_{\mathrm{NL}}\rangle$ scales as $L^{0.7}$, a slightly stronger dependence than in systems using a fixed polarization multiplexed quadrature phase-shift keying (PM-QPSK) constellation [3], where the dependence was found to be $L^{0.45}$. In the dispersion-uncompensated system, the $L^{0.85}$ dependence is consistent with [11], where the optimized power was found to be roughly independent of L.

We consider several different measures of SNR and compare these to an equivalent SNR corresponding to the information bit rate achieved by the proposed rate-adaptive scheme. This discussion makes reference to Fig. 11(a) and (b), which describes dispersion-compensated and -uncompensated systems, respectively.

The uppermost solid curves in Fig. 11(a) and (b) show SNR_{AWGN}, which is an empirical estimate of the SNR per symbol (in two polarizations) as limited only by accumulated optical amplifier noise:

$$SNR_{\mathrm{AWGN}} = \frac{P_t}{P_n}. \tag{8}$$

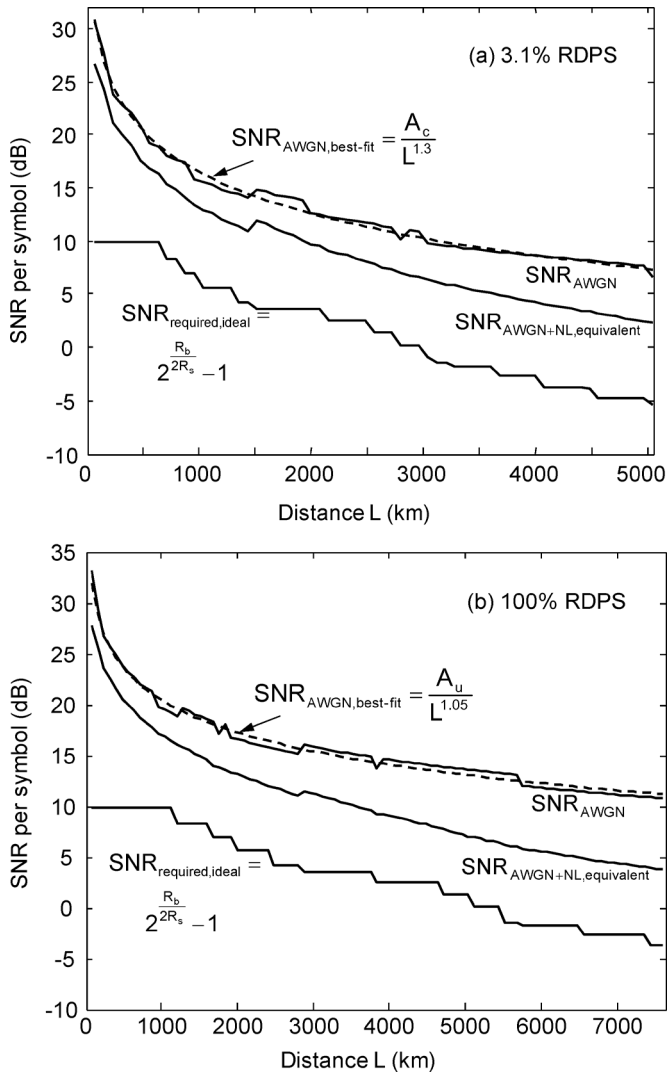

Fig. 11. Different measures of SNR compared to the SNR required for an ideal capacity-achieving coding scheme to achieve error-free transmission at the information bit rate R_b achieved by the proposed rate-adaptive scheme. (a) Dispersion-compensated system. (b) Dispersion-uncompensated system.

Here, P_t is the transmitted signal power, optimized at each transmission distance without repetition encoding ($f_R = 1$), which equals the received signal power at the demultiplexer input, since the network is designed to have unit signal gain. P_n is the noise power in two polarizations and is computed using [3, eq. (8)]. In general, the noise power P_n is proportional to the number of amplifiers traversed [12], so it scales linearly with distance, $P_n \propto L$. The dashed curves in Fig. 11(a) and (b) show $SNR_{\mathrm{AWGN,best-fit}}$ for dispersion-compensated and dispersion-uncompensated systems, respectively, which is a power-law fit to the observed SNR_{AWGN} as a function of transmission distance L:

$$SNR_{\mathrm{AWGN,\ best-fit}} = \begin{cases} \frac{A_c}{L^{1.30}}, & 3.1\%\ \mathrm{RDPS} \\ \frac{A_u}{L^{1.05}}, & 100\%\ \mathrm{RDPS}. \end{cases} \tag{9}$$

The constant A_c, A_u and the exponents of L have been found by curve fitting. In the dispersion-compensated system, SNR_{AWGN} scales as $L^{-1.30}$, a slightly weaker dependence than in systems using a fixed PM-QPSK constellation [3], where the dependence was found to be $L^{-1.55}$. In the dispersion-uncompensated system, the $L^{-1.05}$ dependence is consistent with [11], where the optimized SNR was found to scale as L^{-1}. Considering the dependencies of $\langle \phi_{\mathrm{NL}} \rangle$ and P_n on L through the relationship $\langle \phi_{\mathrm{NL}} \rangle \propto P_t L$ [13], the power laws in (7) and (9) are consistent.

The middle solid curves in Fig. 11(a) and (b) show $SNR_{\mathrm{AWGN\ +\ NL,\ equivalent}}$ for dispersion-compensated and dispersion-uncompensated systems, respectively, which is the SNR per symbol observed empirically at the derepeater input, and includes all effects of amplifier noise and fiber nonlinearity ("equivalent" refers to the fact that their sum may not be Gaussian-distributed). At small L, $SNR_{\mathrm{AWGN\ +\ NL,\ equivalent}}$ is about 2.6 and 2.7 dB lower than SNR_{AWGN} for dispersion-compensated and dispersion-uncompensated systems, respectively, indicating that at the optimum P_t, amplifier noise and nonlinear noise powers are approximately equal, while at large L, the difference increases to about 4.3 and 7.0 dB for dispersion-compensated and dispersion-uncompensated systems, respectively, presumably because significant ROADM channel narrowing over long distances causes equalizer noise enhancement.

The bottom solid curves in Fig. 11(a) and (b), $SNR_{\mathrm{required,\ ideal}}$, are computed by inverting the formula for the capacity of a ideal discrete-time AWGN channel transmitting at symbol rate R_s in two polarizations, i.e., $C = 2R_s \log_2(1 + SNR)$:

$$SNR_{\mathrm{required,\ ideal}} = 2^{\frac{R_b}{2R_s}} - 1. \tag{10}$$

$SNR_{\mathrm{required,\ ideal}}$ corresponds to the SNR required for an ideal, capacity-achieving coding scheme to achieve error-free transmission at the information bit rate R_b achieved by the proposed scheme with zero SNR margin in Fig. 9. The vertical separation between $SNR_{\mathrm{AWGN\ +\ NL,\ equivalent}}$ and $SNR_{\mathrm{required,\ ideal}}$ is an estimate of the performance gap between an ideal rate-adaptive scheme and the scheme proposed here. For dispersion-compensated systems, the gap ranges from about 6.4 to about 7.6 dB as L varies from 640 to 5040 km. For dispersion-uncompensated systems, the gap ranges from about 6.6 to about 7.5 dB as L varies from 1120 to 7600 km. Much of the increase in the gap arises from the inefficiency of the repetition coding used beyond 3280 and 5760 km for dispersion-compensated and dispersion-uncompensated systems, respectively. We expect that some, but not all, of this gap can be closed by using more powerful FEC codes.

We now discuss requirements placed on laser linewidths by the proposed rate-adaptive scheme. We evaluated linewidth requirements including equalization-enhanced phase noise effects for both dispersion-compensated and dispersion-uncompensated systems using the results of [14] and [15]. We assume the system will be designed so that all phase noise effects cause a 1-dB penalty, and that to accommodate this penalty, the transmission mode (M, f_R, r_C) is chosen to provide a margin of 1 dB at each transmission distance, as specified in Fig. 9. We assume identical linewidths for the transmitter and local oscillator. We find that the narrowest linewidth requirements are at the shortest distances, where 16-QAM is used. These requirements are about 2.6 MHz and 800 kHz

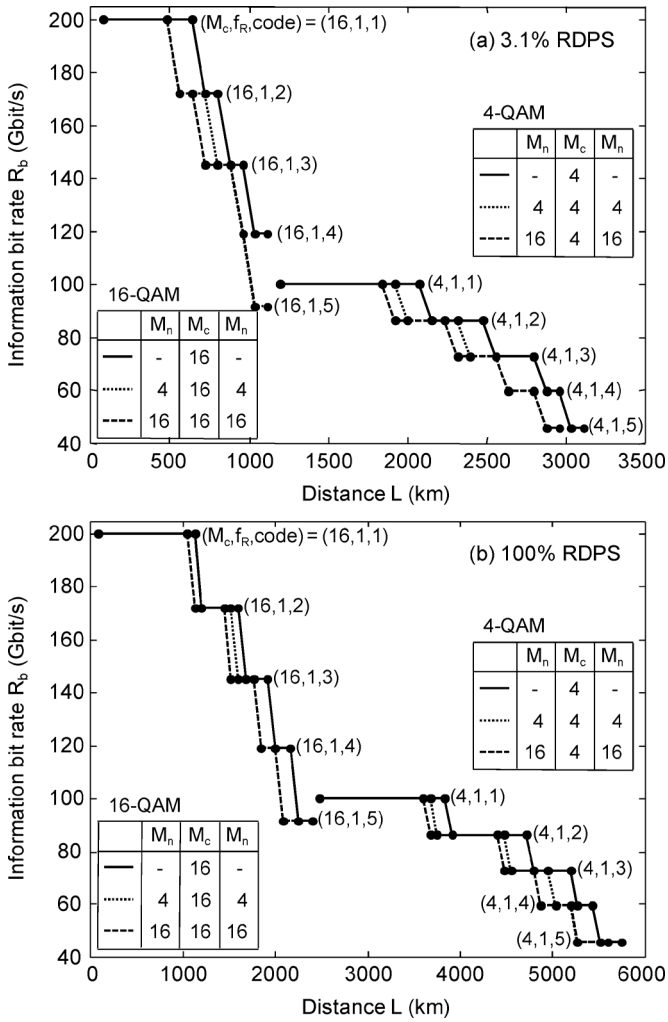

Fig. 12. Achievable information bit rates versus transmission distance with zero SNR margin, comparing one- and three-channel transmission systems. The set $(M_c, f_R, \mathrm{code})$ denotes the modulation order, repetition factor and type of RS–RS code for the center channel, and M_n denotes the modulation order for the neighboring channels, when present. (a) Dispersion-compensated system. (b) Dispersion-uncompensated system.

for dispersion-compensated and dispersion-uncompensated systems, respectively, which can be met using commercially available lasers, such as distributed feedback devices with linewidths less than 200 kHz [16].

Timing recovery should be designed carefully to yield acceptably small jitter at the extremely low operating SNRs enabled by the proposed rate-adaptive scheme.

Finally, we discuss three-channel simulations to evaluate the impact of interchannel nonlinearities in WDM systems. Based on [17], we estimate that simulating a dense WDM system with k channels increases required simulation time by $k^{3.5}$. For $k = 3$, this corresponds to a factor of 46.8, so we have performed a limited number of three-channel simulations. We studied only $M = 4$ and 16, and $f_R = 1$, considering various combinations of modulation orders for the center (M_c) and neighboring (M_n) channels: $[M_n, M_c, M_n] = [4,4,4], [16,4,16], [4,16,4]$, and $[16,16,16]$. In single-channel transmission, optimal transmit power levels for 4-QAM are 1 and 0 dB higher than those for 16-QAM in dispersion-compensated and dispersion-uncompensated systems, respectively. We maintain these power-level ratios in three-channel simulations and optimize the transmit power as described in Section IV. Optimized transmit powers for three-channel transmission are 1 dB lower than for single-channel transmission for both 4- and 16-QAM in both dispersion-compensated and dispersion-uncompensated systems.

Employing the rate adaptation algorithm of Section II-C, Fig. 12(a) and (b) shows achievable information bit rates with zero SNR margin as a function of transmission distance, with and without inline dispersion compensation, respectively, comparing one- and three-channel systems. We observe that in three-channel systems, for a given information bit rate, maximum transmission distances are decreased by 1–3 spans and 2–5 spans in dispersion-compensated and dispersion-uncompensated systems, respectively. These distance reductions correspond to about 10% and 7% for dispersion-compensated and dispersion-uncompensated systems, respectively. We note that the distance reduction is slightly worse when neighboring channels use 16-QAM, which is not a constant-envelope modulation scheme. We expect that qualitatively similar results would be obtained for all modulation orders, repetition factors, and SNR margins, or including a larger number of neighboring channels. We caution, however, that much greater performance degradation is expected when neighboring channels use certain legacy modulation schemes, such as 10 Gb/s NRZ [18] or as the number of neighboring channel increases [19]. Multichannel simulations could be sped up significantly using graphics processing unit-based methods [20].

VI. Conclusion

We have studied a rate-adaptive transmission scheme using variable-rate FEC codes, variable signal constellations, and a fixed symbol rate. The FEC scheme employs serially concatenated RS codes with hard-decision decoding, using shortening and puncturing to vary the code rate. An inner repetition code with soft combining provides further rate variation. We have combined the FEC scheme with single-carrier PM-M-QAM with varying M and digital coherent detection, evaluating performance in a model long-haul system with and without inline dispersion compensation. With zero SNR margin, the information bit rates of 200/100/50 Gb/s are achieved over distances of 640/2080/3040 and 1120/3760/5440 km for dispersion-compensated and dispersion-uncompensated systems, respectively. Compared to an ideal coding scheme achieving information-theoretic limits on an AWGN channel, the proposed scheme exhibits a performance gap ranging from about 6.4 dB at 640 km to 7.6 dB at 5040 km for dispersion-compensated system, and from about 6.6 dB at 1120 km to 7.5 dB at 7600 km for dispersion-uncompensated system. Much of the increase in the gap can be attributed to suboptimality of the repetition coding used beyond 3280 and 5760 km for dispersion-compensated and dispersion-uncompensated systems, respectively. We found that the SNR as limited by amplifier noise scales with distance L as $L^{-1.30}$ and $L^{-1.05}$ for dispersion-compensated and dispersion-uncompensated systems, respectively. In three-channel systems, interchannel nonlinearities decrease achievable distances by about 10% and 7% for dispersion-compensated and dispersion-uncompensated systems, respectively.

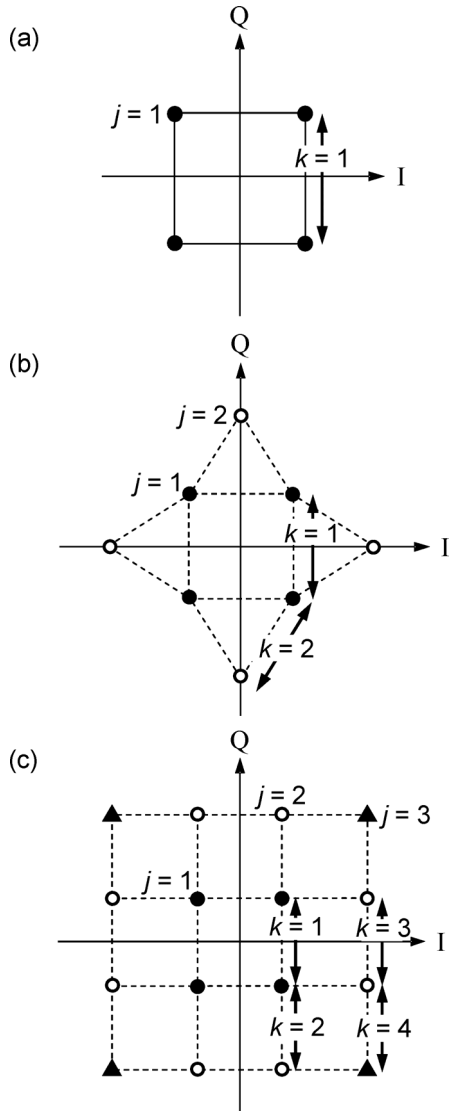

Fig. 13. Different classes of constellation points and Q factors. (a) 4-QAM: one class of points and one class of constellation point pairs. (b) 8-QAM: two classes of points and two classes of pairs. (c) 16-QAM: three classes of points and four classes of pairs.

APPENDIX

In this appendix, we discuss methods to compute error probabilities. All quantities considered here are measured at the derepeater output (in the case $f_R = 1$, all quantities are the same at the derepeater input). As described in Section II-A, we assume Gray mapping for $M = 4, 16$ or the mapping of [4] for $M = 8$, so the BER $P_{b,\text{in}}$ and SER $P_{s,\text{in}}$ are related by (3). A constellation with M points can be divided into J equivalence classes of points, denoted by $j = 1, \ldots, J$, where class j includes M_j points. The constellation can also be described as including K equivalence classes of pairs of points, denoted by $k = 1, \ldots, K$. This notation for points and pairs of points is illustrated in Fig. 13. Values of the parameters for constellations with $M = 4, 8, 16$ are given in Table II.

Suppose the minimum distance between in a constellation is d. Let N_{jk} denote the number of nearest neighbors at distance d with which a point in class j forms pairs in class k.

TABLE II
CLASSES OF CONSTELLATION POINTS AND Q FACTORS. THE NOTATION IS DEFINED IN THE TEXT

M	J	K	j	M_j	k for $N_{jk} \neq 0$	N_{jk}
4	1	1	1	4	1	2
8	2	2	1	4	1	2
					2	2
			2	4	2	2
16	3	4	1	4	1	2
					2	2
			2	8	2	1
					3	1
					4	1
			3	4	4	2

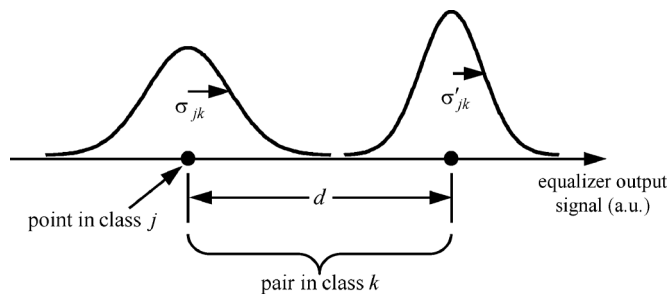

Fig. 14. Conditional probability densities of received signal (at equalizer output) along a line joining a point in class j with a neighbor with which it forms a pair in class k.

Fig. 14 shows the conditional probability densities of the received signal (at the equalizer output) along the line joining a point with its neighbor. Let σ_{jk} be the ensemble-average standard deviation of the total "noise" (including residual ISI and nonlinearity) on the point in class j, and let σ'_{jk} denote the corresponding quantity on the neighboring point. Assuming the decision threshold is set midway between the points (as in our implementation), assuming the total "noise" is Gaussian, the ensemble-average SER for a point in class j can be approximated as

$$P_{s,\text{in},j} \approx \sum_{k=1}^{K} N_{jk} Q\left(\frac{d}{2\sigma_{jk}}\right). \tag{11}$$

If σ_{jk} and σ'_{jk} are unequal (as indicated in Fig. 14), the error probability can be minimized by setting the threshold at a distance $(\sigma_{jk})/(\sigma_{jk} + \sigma'_{jk})d$ from the point in class j. Defining a Q factor for the pair of class k:

$$Q_k = \frac{d}{\sigma_{jk} + \sigma'_{jk}} \tag{12}$$

the SER for the point in class j is approximated as

$$P_{s,\text{in},j} \approx \sum_{k=1}^{K} N_{jk} Q(Q_k). \tag{13}$$

In any case, the average SER is given by

$$P_{s,\mathrm{in}} = \frac{1}{M}\sum_{j=1}^{J} M_j P_{s,\mathrm{in},j}. \tag{14}$$

Note that in the AWGN case, for a given constellation, all σ_{jk} and σ'_{jk} become equal, all Q_k become equal, and (11) and (14) [or (13) and (14)] become equivalent to (2).

To test the accuracy of our error-probability analysis, after propagating signals through our nonlinear fiber network, we estimated the standard deviation of the total "noise" on each constellation point. As a first test, we computed $P_{s,\mathrm{in},j}$ using (11), and employed (14) and (3) to compute $P_{b,\mathrm{in}}$. We then compared the results to $P_{b,\mathrm{in}}$ measured by error counting. For $M = 4$, predicted and measured values of $P_{b,\mathrm{in}}$ agreed within 0.18 dB, as in [3]. For $M = 8, 16$, measured values exceeded computed values by factors corresponding to 0.56 and 0.38 dB, respectively. As a second test, we computed the Q_k using (12), and employed (13), (14) and (3) to predict $P_{b,\mathrm{in}}$. Compared to values of $P_{b,\mathrm{in}}$ measured by error counting, we observed the same errors (within 0.01 dB) as with the first method. The $P_{b,\mathrm{in}}$ computation method using (3), (11), and (14) was employed in optimizing the transmit power and estimating $P_{b,\mathrm{in}}$ when the expected $P_{b,\mathrm{in}}$ is very low, as described in Section III.

REFERENCES

[1] J. McDonough, "Moving standards to 100 GbE and beyond," *IEEE Appl. Practice*, vol. 45, no. 11, pp. 6–9, Nov. 2007.

[2] Interfaces for Optical Transport Network, ITU-T G.709 Dec., 2009.

[3] G. Gho, L. Klak, and J. M. Kahn, "Rate-adaptive coding for optical fiber transmission systems," *J. Lightw. Technol.*, vol. 29, no. 2, pp. 222–233, Jan. 2011.

[4] E. Ip and J. M. Kahn, "Carrier synchronization for 3- and 4-bit-per-symbol optical transmission," *J. Lightw. Technol.*, vol. 23, no. 12, pp. 4110–4124, Dec. 2005.

[5] P. K. Vitthaladevuni, M.-S. Alouini, and J. C. Kieffer, "Exact BER computation for cross QAM constellations," *IEEE Trans. Wireless Commun.*, vol. 4, no. 6, pp. 3039–3050, Nov. 2005.

[6] Forward Error Correction for Submarine Systems, ITU-T G.975, Nov., 1996.

[7] Forward Error Correction for High Bit-Rate DWDM Submarine Systems, ITU-T G.975.1, Feb., 2004.

[8] J. G. Proakis, *Digital Communications*, 5th ed. New York: McGraw-Hill, 2007.

[9] E. Ip and J. M. Kahn, "Digital equalization of chromatic dispersion and polarization mode dispersion," *J. Lightw. Technol.*, vol. 25, no. 8, pp. 2033–2043, Aug. 2007.

[10] O. V. Sinkin, R. Holzlöhner, J. Zweck, and C. R. Menyuk, "Optimization of the split-step Fourier method in modeling optical-fiber communications systems," *J. Lightw. Technol.*, vol. 21, no. 1, pp. 61–68, Jan. 2003.

[11] R.-J. Essiambre, G. Kramer, P. J. Winzer, G. J. Foschini, and B. Goebel, "Capacity limits of optical fiber networks," *J. Lightw. Technol.*, vol. 28, no. 4, pp. 662–701, Feb. 2010.

[12] E. Desurvire, *Erbium-Doped Fiber Amplifiers: Principles and Applications*. New York: Wiley, 1994.

[13] G. P. Agrawal, *Fiber-Optic Communication Systems*, 3rd ed. : Wiley, 2002.

[14] E. Ip and J. M. Kahn, "Feed-forward carrier recovery for coherent optical communications," *J. Lightw. Technol.*, vol. 25, no. 9, pp. 2675–2692, Sep. 2007.

[15] W. Shieh and K.-P. Ho, "Equalization-enhanced phase noise for coherent-detection systems using electronic digital signal processing," *Opt. Exp.*, vol. 16, no. 20, pp. 15718–15727, Sep. 2008.

[16] J. P. Wilde, G. W. Yoffe, and J. M. Kahn, "Frequency noise characterization of a widely tunable narrow-linewidth DFB laser array source," presented at the presented at the Opt. Fiber Commun. Conf., San Diego, CA, Mar. 22–26, 2009.

[17] Q. Zhang and M. I. Hayee, "Symmetrized split-step Fourier scheme to control global simulation accuracy in fiber-optic communication systems," *J. Lightw. Technol.*, vol. 26, no. 2, pp. 302–316, Jan. 2008.

[18] O. Bertran-Pardo, J. Renaudier, G. Charlet, H. Mardoyan, P. Tran, and S. Bigo, "Nonlinearity limitations when mixing 40-Gb/s coherent PDM-QPSK channels with preexisting 10-Gb/s NRZ channels," *IEEE Photon. Technol. Lett.*, vol. 20, no. 15, pp. 1314–1316, Aug. 2008.

[19] C. Xia and D. van den Borne, "Impact of the channel count on the nonlinear tolerance in coherently-detected POLMUX-QPSK modulation," presented at the presented at the Opt. Fiber Commun. Conf./Nat. Fiber Opt. Eng. Conf., Los Angeles, CA, Paper OWO1.

[20] S. Pachnicke, A. Chachaj, M. Helf, and P. M. Krummrich, "Fast parallel simulation of fiber optical communication systems accelerated by a graphics processing unit," presented at the presented at the Int. Conf. Transp. Opt. Netw., Munich, Germany, 2010, Paper Th.B1.5.

Gwang-Hyun Gho received the B.S. degree in electronics engineering from Korea University, Seoul, Korea, in 1995, and the M.S. and Ph.D. degrees in electrical engineering from Stanford University, Stanford, CA, in 1999 and 2011, respectively.

From 1999 to 2005, he was at Qualcomm Inc., Campbell, CA, where he developed WCDMA and HSDPA modems as a Systems Engineer. From 2005 to 2009, he was a DSP engineer at Amicus Wireless Technology Inc., Sunnyvale, CA, developing mobile WiMAX modem. Since 2011, he has been developing LTE modem at Qualcomm Inc., Santa Clara, CA, as a Firmware Engineer. His research interests include optical and wireless communications, error control coding, and digital signal processing.

Joseph M. Kahn (M'90–SM'98–F'00) received the A.B., M.A., and Ph.D. degrees in physics from the University of California, Berkeley, in 1981, 1983, and 1986, respectively.

From 1987 to 1990, he was at AT&T Bell Laboratories, Crawford Hill Laboratory, Holmdel, NJ. He demonstrated multi-Gb/s coherent optical fiber transmission systems, setting world records for receiver sensitivity. From 1990 to 2003, he was on the Faculty of the Department of Electrical Engineering and Computer Sciences, University of California, Berkeley, performing research on optical and wireless communications. Since 2003, he has been a Professor of electrical engineering at Stanford University, Stanford, CA. His current research interests include single-mode and multimode optical fiber communications, free-space optical communications, and microelectromechanical systems for optical communications. In 2000, he helped found StrataLight Communications, where he has served as the Chief Scientist from 2000 to 2003. StrataLight (now Opnext Subsystems) is a leading supplier of transmission subsystems for high-capacity terrestrial networks.

Dr. Kahn received the National Science Foundation Presidential Young Investigator Award in 1991. From 1993 to 2000, he has served as a Technical Editor of IEEE PERSONAL COMMUNICATIONS MAGAZINE. Since 2009, he has been an Associate Editor of the IEEE/OSA JOURNAL OF OPTICAL COMMUNICATIONS AND NETWORKING.